

Kramers Nonlinearity in PT Symmetric Magnets

Oles Matsyshyn, Ying Xiong and Justin C. W. Song

¹*Division of Physics and Applied Physics, School of Physical and Mathematical Sciences, Nanyang Technological University, Singapore 637371,*

Kramers degeneracies play an essential role in the spectrum of electronic materials. Here we argue that beyond spectral properties, Kramers degeneracy plays a critical role in the nonlinear response of PT symmetric magnets. In particular, we uncover a class of second-order Kramers nonlinearities that only arise in the presence of Kramers degeneracy, vanishing in non-degenerate PT symmetric materials. Kramers nonlinearities depend on a circular dichroism between PT related Kramers states and enable to trace out the quantum geometry of the degenerate band structure. We find pronounced Kramers nonlinearities in the nonlinear polarization responses of even layer antiferromagnetic MnBi₂Te₄ that enable to identify its antiferromagnetic order. This provides novel means for diagnosing Kramers pairs and addressing the internal Kramers degree of freedom.

PACS numbers: 72.15.-v,72.20.My,73.43.-f,03.65.Vf

Introduction. Spin and its transformation properties under time reversal (T) place strong constraints on electronic states. A case in point are Kramers degeneracies: in the presence of T-symmetry, states with odd half-integer spin occur in orthogonal pairs with the same energy. Such Kramers pairs play a critical role in determining the electronic properties of quantum materials, e.g., it ensures the gapless nature of edge states in T-invariant topological insulators [1]. Interestingly, Kramers pairs can persist even in magnetic materials. When both T and inversion, P, symmetries are broken but their composite PT-symmetry is preserved, Kramers degeneracies survive with each electronic Bloch state at least doubly degenerate [2, 3]. Such Kramers pairs form a PT-protected internal degree of freedom [4].

Here we argue that Kramers degeneracy play a critical role in nonlinear response [5–12]. We introduce *Kramers nonlinearities*: second-order nonlinearities to an incident electromagnetic field that depend on the presence of Kramers degeneracy in PT-symmetric materials. Kramers nonlinearities only arise in the presence of Kramers degeneracy and *vanish* for non-degenerate energy bands in PT-invariant systems. This unusual defining feature makes Kramers nonlinearities a powerful diagnostic of Kramers degeneracy in PT-symmetric magnets that go beyond spectral features [3].

At the heart of Kramers nonlinearities is the ability to access contrasting behavior of the states in each Kramers pair [2]. PT-even observables such as (the well-studied) charge current possess the same expectation value for both states in each Kramers pair. In contrast, PT-odd observables (e.g., electric polarization, magnetization, or spin polarization) possess distinct values for states in each Kramers pair. Odd parity under PT ensures such (PT-odd) observables are compensated within each Kramers pair. In non-degenerate energy bands, the constraint is stronger: material PT-invariance guarantees that the expectation value of PT-odd observables in each electronic state vanishes. Our work shows that when coherent optical transitions between degenerate electronic bands imbalance Kramers pairs (Fig. 1), PT-odd observ-

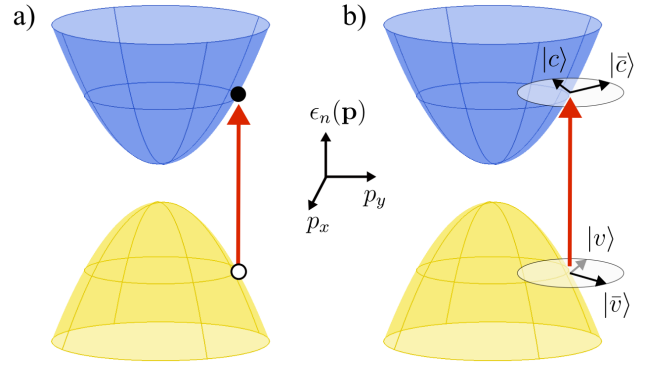


FIG. 1: *Kramers Pair Optical Transitions.* (a) Optical interband absorption for non-degenerate electronic energy bands can be tracked by following the energy and momentum conserving transition of an electron in a non-degenerate electronic state in the valence band to an unoccupied non-degenerate electronic state in the conduction band. (b) In contrast, the optical interband process in degenerate electronic bands involve tracking the wavefunction amplitudes of Kramers *pairs* of degenerate states from (v, \bar{v}) to (c, \bar{c}) . Such paired transitions are critical in activating nonlinear responses in PT symmetric electronic materials.

ables become activated switching on Kramers nonlinearities. As a result, Kramers nonlinearities are chiral and enable to probe the quantum geometry of Bloch states [11–20] in Kramers degenerate bands.

Our work is situated in a current surge of interest in PT symmetric magnetic materials and devices [3, 4, 21–24]. While often treated as a spectator degree of freedom, we find Kramers pairs are essential to pronounced second order nonlinearities that readily manifest in a range of PT-symmetric magnetic materials. For instance we find even layered MnBi₂Te₄ [4, 21] antiferromagnets can realize pronounced Kramers nonlinearity such as a light-induced nonlinear layer polarization that can be switched by both helicity as well as the underlying Néel order. This illustrates how Kramers nonlinearities are a powerful means of controlling the layer degree of freedom and

probing the underlying antiferromagnetic order in quantum materials.

Injection nonlinearity and Kramers pair transitions.

Key to optical interband nonlinearities are optical transitions between bands. In materials with non-degenerate energy bands, interband second-order nonlinearities are driven by optical absorption and depend directly on the rate of interband optical transitions. A striking example is the injection nonlinearity. For an observable O , interband optical transitions of an electron from valence band v to conduction band c (see Fig. 1) induces a change in its expectation value. Since transitions occur at rate $W_{v \rightarrow c}$, this process produces the familiar form of the injection nonlinearity in non-degenerate energy bands [7–12, 25, 26]

$$\frac{dO}{dt} = \sum_{v \rightarrow c} [O_{cc}(\mathbf{p}) - O_{vv}(\mathbf{p})] f_{cv}(\mathbf{p}) W_{v \rightarrow c}(\mathbf{p}), \quad (1)$$

where $O_{nm}(\mathbf{p}) = \langle n, \mathbf{p} | \hat{O} | m, \mathbf{p} \rangle$ is the matrix element between state $\{n, \mathbf{p}\}$ and state $\{m, \mathbf{p}\}$ for an operator \hat{O} , and $f_{cv}(\mathbf{p}) = f[\epsilon_c(\mathbf{p})] - f[\epsilon_v(\mathbf{p})]$ is the difference of Fermi functions in conduction and valence bands with $\epsilon_n(\mathbf{p})$ the energy of state with momentum \mathbf{p} in band n . For a monochromatic electromagnetic field $\mathbf{E}(t) = (\mathbf{E}_\omega e^{-i\omega t} + c.c.)/2$, the transition rate can be written in terms of the dipole matrix elements of the interband position operator $r_{vc}^\alpha = A_{vc}^\alpha = \langle v, \mathbf{p} | i\partial_{\mathbf{p}}^\alpha | c, \mathbf{p} \rangle$, where A^α is the Berry connection, as $W_{v \rightarrow c}(\mathbf{p}) = (2\pi/\hbar) r_{vc}^\alpha(\mathbf{p}) r_{cv}^\beta(\mathbf{p}) e^2 E_{-\omega}^\alpha E_\omega^\beta \delta[\hbar\omega - \epsilon_c(\mathbf{p}) + \epsilon_v(\mathbf{p})]$.

This direct dependence on the interband transition rate in Eq. (1) can be exploited to interrogate the geometry of optical transitions described by $r_{vc}^\alpha(\mathbf{p})$ [9, 11]. For instance, when $\hat{O} = e\hat{\mathbf{v}}$ is the charge photocurrent (a PT-even observable), Eq. (1) describes the injection photocurrent that can track the Berry flux of Weyl semimetals [8, 27] and an interband quantum metric dipole in noncentrosymmetric magnets [9, 12].

No less striking are observables that are odd under PT: $\mathbf{PT}\hat{O}^{(-)}(\mathbf{PT})^{-1} = -\hat{O}^{(-)}$ that include polarization or spin magnetization. While such observables produce large second-order injection nonlinearities in T symmetric materials [28, 29], for PT symmetric non-degenerate energy bands, $O_{nn}^{(-)} = 0$ in Eq. (1). This zeroes the injection nonlinearity for $O^{(-)}$ in non-degenerate PT systems even as the interband transition rate $W_{v \rightarrow c}$ is finite.

As we now explain, degeneracy can drastically change the nonlinear dynamics of $O^{(-)}$. We proceed by analyzing a Bloch Hamiltonian $H_0(\mathbf{p})$ with Bloch eigenstates $|u_n(\mathbf{p})\rangle$ and energy $\epsilon_n(\mathbf{p})$. Materials with PT symmetry, $\mathbf{P}\mathbf{T}H_0(\mathbf{p})(\mathbf{P}\mathbf{T})^{-1} = H_0(\mathbf{p})$, ensures that electrons (odd spin-half particles) occur in doubly-degenerate Kramers pairs at every \mathbf{p} : there exist two orthogonal states $|u_n(\mathbf{p})\rangle$ and $|u_{\bar{n}}(\mathbf{p})\rangle$ with $\epsilon_n(\mathbf{p}) = \epsilon_{\bar{n}}(\mathbf{p})$. Interestingly, such PT symmetry enforced Kramers degeneracy place strong constraints on the matrix elements.

$$O_{nn}^{(\pm)}(\mathbf{p}) = \pm O_{\bar{n}\bar{n}}^{(\pm)}(\mathbf{p}), \quad O_{n\bar{n}}^{(\pm)}(\mathbf{p}) = \mp O_{\bar{n}n}^{(\pm)}(\mathbf{p}), \quad (2)$$

where (\pm) superscript indicate observables that are PT even (odd) respectively. Importantly, for PT-odd observables, both $O_{nn}^{(-)}$ and $O_{\bar{n}\bar{n}}^{(-)}$ can be nonzero. As we argue below, Eq. (2) together with the optical transitions of Kramers pairs lead to finite injection nonlinearities for $O^{(-)}$ observables even in the presence of PT symmetry.

To see this, we examine light-induced transitions from a valence to conduction band. For non-degenerate electronic bands, such transitions involve two states only: $|u_v(\mathbf{p})\rangle$ and $|u_c(\mathbf{p})\rangle$ (see Fig. 1a). In contrast, optical transitions in Kramers degenerate systems inevitably involve four states: from valence band $\{|u_v(\mathbf{p})\rangle, |u_{\bar{v}}(\mathbf{p})\rangle\}$ subspace to conduction band $\{|u_c(\mathbf{p})\rangle, |u_{\bar{c}}(\mathbf{p})\rangle\}$ subspace (see Fig. 1b). Here we have anticipated energy and momentum conservation. To appreciate this, first consider an electron initially in the state $|u_v(\mathbf{p})\rangle$ only. Light induces dynamics so that its quantum state can be described as a superposition of both Kramers pairs:

$$|\Psi(t)\rangle = \sum_{i \in v, \bar{v}} s_i(t) |u_i(\mathbf{p})\rangle + \sum_{j \in c, \bar{c}} s_j(t) |u_j(\mathbf{p})\rangle, \quad (3)$$

where $s_{i,j}(t)$ are amplitudes in the Kramers degenerate subspaces of the valence and conduction band respectively and can be computed in the standard iterative fashion for light-matter interaction $\hat{V}(t) = e\mathbf{E}(t) \cdot \hat{\mathbf{r}} e^{\eta t/\hbar}$ with $\eta \rightarrow 0^+$ an adiabatic turn-on parameter, see Supplementary Information, SI.

Interestingly, the optical transition process in Kramers degenerate bands described in Eq. (3) cannot be understood as a simple sum of transitions in two independent sets of non-degenerate bands. For example, even as the electron was initialized in $|u_v(\mathbf{p})\rangle$ only, light induces a non-zero amplitude in its Kramers pair $|u_{\bar{v}}(\mathbf{p})\rangle$ with a transition amplitude $s_{\bar{v}}(t)$ that goes as $r_{\bar{v},c}(\mathbf{p})r_{c,v}(\mathbf{p}) + r_{\bar{v},\bar{c}}(\mathbf{p})r_{\bar{c},v}(\mathbf{p})$. This involves matrix elements across *three* distinct states. As a result, Kramers pair optical transitions are readily understood to occur from one degenerate (valence) subspace to another degenerate (conduction) subspace.

Using Eq. (3), we directly compute the injection nonlinearity for Kramers degenerate systems by examining its expectation value $\langle O \rangle = \langle \psi(t) | \hat{O} | \psi(t) \rangle$ summed over all possible initial and final (v, \bar{v}, c, \bar{c}) states to order V^2 . Focussing on the rectified contribution, we find

$$\frac{dO}{dt} = \frac{\pi e^2}{2\hbar} \sum_{\substack{mn \\ \zeta=\pm 1}} \delta(\epsilon_{mn} - \zeta\hbar\omega) r_{nm}^\alpha \mathbb{O}_{mn}^\beta f_{nm} E_{-\zeta\omega}^\alpha E_{\zeta\omega}^\beta, \quad (4)$$

where $\mathbb{O}_{mn}^\beta = \sum_{i, \epsilon_i = \epsilon_m} O_{mi} r_{in}^\beta - \sum_{j, \epsilon_j = \epsilon_n} O_{jn} r_{mj}^\beta$ captures a three-state coherent process involved in the Kramers optical transition. Several comments are in order.

First, and most strikingly, Eq. (4) produces a non-vanishing injection nonlinearity for $O = O^{(-)}$, even for PT symmetric materials [i.e. satisfying Eq. (2)]. We term these *Kramers nonlinearities* since such nonlinearities manifest due to the presence of Kramers degeneracy; it vanishes for a non-degenerate PT symmetric sys-

tem. Indeed, Kramers nonlinearities arise due to a light-induced imbalancing of Kramers pairs. To see this, we note that for PT systems $\mathbb{O}_{mn}^\beta r_{nm}^\alpha = \mathbb{O}_{\bar{n}\bar{m}}^\beta r_{\bar{m}\bar{n}}^\alpha$. Yielding Eq. (4) is proportional to $[\mathbf{E}_{-\omega} \times \mathbf{E}_\omega]$, see **SI**. This demonstrates the Kramers nonlinearity in Eq. (4) arises only for circularly polarized light. Indeed, it captures a circular dichroism of PT related Kramers states. For PT symmetric materials, linearly polarized light or the absence of degeneracy zeroes such dichroism.

Finally, we note that Eq. (4) is general: for $O = O^{(+)}$ and applying Eq. (2), we find Eq. (4) reduces to the familiar Eq. (1). In contrast, when $O = O^{(-)}$, Eq. (4) departs from Eq. (1). In particular, Eq. (4) cannot be factorized into a product of the interband transition rate and an expectation value since it involves a three-state coherent process (see \mathbb{O}_{mn}^β above). Such three-state processes do not occur for injection nonlinearities of $O^{(+)}$ since $O_{n\bar{n}}^{(+)} = 0$ [see Eq. (2)]. Off-diagonal $O_{n\bar{n}}^{(-)}$, on the other hand, are in general non-zero for PT-odd observables and are essential to guarantee the U(2) gauge invariance of Kramers nonlinearities in Eq. (4).

Kramers nonlinearities and quantum geometry. Photocurrent nonlinearities (nonlinearities of PT-even observables) are well-known to depend on the quantum geometry of Bloch states involved in optical transitions [9, 11, 18–20, 30, 31]. As we now argue, nonlinearities of PT-odd observables also track the geometry of quantum states.

To extract this geometrical connection, we examine the set of Hamiltonians: $H_{\text{eff}}(\lambda, \mathbf{p}) = H_0(\mathbf{p}) + \lambda \hat{O}^{(-)}$ parameterized by λ with Bloch eigenenergies $\varepsilon_n(\mathbf{p}, \lambda)$ and eigenstates $|\mathfrak{u}_n(\mathbf{p}, \lambda)\rangle$. Writing $\hat{O}^{(-)} = \partial_\lambda H_{\text{eff}}$ produces an identity for $\tilde{O}_{nm}^{(-)}(\mathbf{p}, \lambda) = \langle \mathfrak{u}_n(\mathbf{p}, \lambda) | \hat{O}^{(-)} | \mathfrak{u}_m(\mathbf{p}, \lambda) \rangle$:

$$\tilde{O}_{nm}^{(-)}(\mathbf{p}, \lambda) = \partial_\lambda \varepsilon_n(\mathbf{p}, \lambda) \delta_{nm} + i \varepsilon_{nm}(\mathbf{p}, \lambda) \mathcal{A}_{nm}^\lambda(\mathbf{p}, \lambda), \quad (5)$$

where $\varepsilon_{nm}(\mathbf{p}, \lambda) = \varepsilon_n(\mathbf{p}, \lambda) - \varepsilon_m(\mathbf{p}, \lambda)$, and the λ -Berry connection is $\mathcal{A}_{nm}^\lambda = \langle \mathfrak{u}_n(\mathbf{p}, \lambda) | i \partial_\lambda | \mathfrak{u}_m(\mathbf{p}, \lambda) \rangle$. While $\lambda \neq 0$ breaks PT symmetry thereby lifting degeneracy, $H_{\text{eff}}(\lambda \rightarrow 0, \mathbf{p}) = H_0(\mathbf{p})$ restores its Kramers pairs. In what follows, we will take $\lambda \rightarrow 0$ in our final expressions so that $\tilde{O}_{nm}^{(-)}(\mathbf{p}, \lambda \rightarrow 0) = O_{nm}^{(-)}(\mathbf{p})$, with energies $\varepsilon_n(\mathbf{p}, \lambda \rightarrow 0) = \varepsilon_n(\mathbf{p})$ and Bloch states $|\mathfrak{u}_m(\mathbf{p}, \lambda \rightarrow 0)\rangle = |u_m(\mathbf{p})\rangle$. Importantly, geometrical phases accrued in \mathcal{A}_{nm}^λ persist even as $\lambda \rightarrow 0$, enabling to characterize $O^{(-)}$ nonlinearities with the quantum geometry of its states.

We proceed by systematically enumerating the second-order nonlinearities of PT-odd observables $O^{(-)}$. To do so we employ the standard quantum Liouville treatment of nonlinear response [6, 7, 32] but generalized to PT symmetric degenerate bands, see **SI** for full details. Here we report the main results for Kramers induced second-order nonlinear susceptibilities of $\langle O^{(-)} \rangle = e^2 \int d\omega E_{-\omega}^\alpha E_\omega^\beta \chi^{\alpha\beta}$.

For an insulator, we find three second-order nonlinearities of PT-odd observables $\hat{O}^{(-)}$ that depend on Kramers degeneracy in PT symmetric systems (see Table 1). The first is the Kramers injection (KI) nonlinearity [discussed above in Eq. (4)]. Using Eq. (5), the Kramers

PT	Degenerate	Non-Degenerate	Equation
Kramers Injection	✓	✗	Eq. (6)
Kramers Fermi Sea	✓	✗	Eq. (8)
Shift-like	✓*	✓	Eq. (S15)

TABLE I: Table of $O^{(-)}$ second-order nonlinearities that contrast responses of Kramers degenerate (spinful) vs non-degenerate (spinless) PT symmetric systems. (*) indicates a response that is altered by Kramers degeneracy, **SI**.

injection nonlinearity can be expressed in a compact geometrical form

$$\chi_{\text{KI}}^{\alpha\beta} = \frac{\tau\pi}{4\hbar} \int_{\mathbf{p}} \sum_{nm} \delta(\varepsilon_{mn} - \hbar\omega) f_{nm} i (v_{nm}^{\alpha;\lambda} \mathcal{A}_{mn}^\beta - v_{nm}^\alpha \mathcal{A}_{mn}^{\beta;\lambda}), \quad (6)$$

where v_{nm}^α is an interband velocity matrix element, and $(; \lambda)$ denotes the generalized derivative

$$L_{mn}^{\alpha;\lambda} = \lim_{\lambda \rightarrow 0} [D_\lambda, \hat{L}^\alpha]_{mn}, \quad D_\lambda = \partial_\lambda - i \mathcal{A}^\lambda \delta^E, \quad (7)$$

of an operator \hat{L}^α (e.g., position or velocity). Note, that $\lim_{\lambda \rightarrow 0} \langle \mathfrak{u}_n(\mathbf{p}, \lambda) | \mathcal{A}^\lambda \delta^E | \mathfrak{u}_m(\mathbf{p}, \lambda) \rangle \equiv \mathcal{A}_{nm}^\lambda \delta_{\varepsilon_n \varepsilon_m}$ and $[\partial_\lambda, \hat{L}]_{mn} \equiv \partial_\lambda L_{mn}$. Importantly, the generalised derivative naturally sums across the degenerate Kramers states: it is U(2) covariant. As a result, when contracted with $v_{nm}^\alpha \mathcal{A}_{nm}^\beta$, it produces a gauge invariant value. Just like other injection nonlinearities, the KI susceptibility in Eq. (6) is extrinsic and depends on an effective relaxation rate τ or pulse-widths in an ultra-fast measurement [20, 27, 33].

Critically, Eq. (6) demonstrates that the Kramers nonlinearities depend on the quantum geometry of the Kramers states associated with the optical transition. Indeed, generalised derivatives often appear when tracking the geometry of subspaces, e.g., in defining the Hermitian connection and curvature [11]. Just as photocurrent nonlinearities probe the geometry of the subspace of states involved in the optical transitions as \mathbf{p} is varied [9, 11, 12, 30], similarly, the Kramers nonlinearities of PT-odd observables are sensitive to the geometry of Kramers pair optical transitions as λ is varied.

The second $O^{(-)}$ Kramers nonlinearity we find is an off-resonant Kramers Fermi sea (KFS) susceptibility that is present even for a filled Fermi sea:

$$\chi_{\text{KFS}}^{\alpha\beta} = \frac{1}{2} \int_{\mathbf{p}} \sum_{nm} f_{nm} i \mathcal{P} \frac{v_{nm}^{\alpha;\lambda} \mathcal{A}_{mn}^\beta - v_{nm}^\alpha \mathcal{A}_{mn}^{\beta;\lambda}}{(\varepsilon_{mn} - \hbar\omega)^2}. \quad (8)$$

Like the Kramers injection nonlinearity, it similarly vanishes in the absence of Kramers degeneracy for PT symmetric systems. To see this, note that for non-degenerate PT symmetric materials the quantity $v_{nm}^{\alpha;\lambda} \mathcal{A}_{mn}^\beta - v_{nm}^\alpha \mathcal{A}_{mn}^{\beta;\lambda}$ when contracted with electric fields becomes proportional to $i \mathcal{A}_{nm}^\alpha \mathcal{A}_{mn}^\beta (O_{nn}^{(-)} - O_{mm}^{(-)})$; since $O_{nn}^{(-)}$ is zero in PT symmetric non-degenerate electronic bands, $\chi_{\text{KFS}}^{\alpha\beta}$ vanishes.

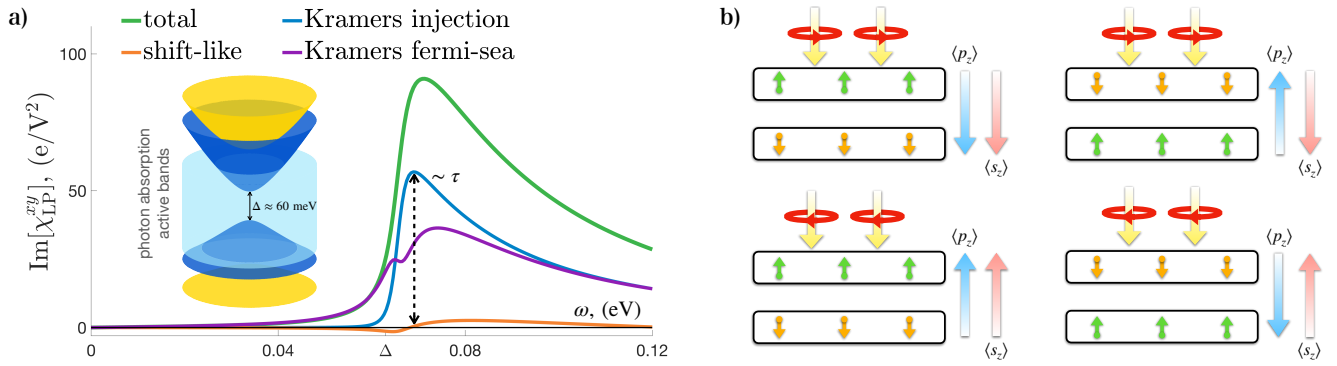


FIG. 2: Kramers nonlinearity in MBT. (a) Helicity dependent non-linear interlayer polarization susceptibility tensor of bilayer MnBi_2Te_4 ($\tau = 0.25\text{ps}$, $\mu = 0.01\text{eV}$, for the complete set of parameters see **SI**). Bilayer MBT band structure (left inset). (b) Schematic illustration of the interlayer polarization and spin responses for distinct circular (LH/RH) polarizations (red circular arrows) and Néel order parameters $x = \pm 1$ (denoted by the green/orange arrows in the bilayer). Here we have denoted positive light-induced $\langle \hat{p}_z \rangle$ and $\langle \hat{s}_z \rangle$ by an up (blue and red) arrow.

In the same fashion as the KI nonlinearity, KFS only arises for circularly polarized light since $\chi_{\text{KI,KFS}}^{\alpha\beta}(\omega) = -\chi_{\text{KI,KFS}}^{\alpha\beta}(-\omega)$ in PT symmetric materials: this makes $\chi_{\text{KI,KFS}}^{\alpha\beta}$ pure imaginary and antisymmetric under $\alpha \leftrightarrow \beta$. In contrast to KI nonlinearity in Eq. (6) above, however, KFS does not require optical absorption and is non-dissipative in nature.

The last $O^{(-)}$ nonlinearity we find in PT symmetric materials are shift-like nonlinearities, see detailed discussion in **SI**. Unlike KI and KFS, such shift-like $O^{(-)}$ nonlinearities persist even in non-degenerate PT symmetric materials. Even as such shift-like nonlinearities do not need Kramers degeneracy to manifest, the presence of Kramers degeneracy nevertheless necessitates modifications to the expressions for shift-like nonlinearities from its naïve non-degenerate form in much the same way as that of gyration photocurrents [9].

Light induced nonlinear polarization in MnBi_2Te_4 . To illustrate Kramers nonlinearities, we examine even-layer MnBi_2Te_4 (MBT): a PT symmetric antiferromagnet. For simplicity, we focus on bilayer MBT; our qualitative conclusions are valid for other even layers. The electronic states of bilayer MBT can be captured by an effective 8-band Hamiltonian [34]: $H_0^{\text{MBT}}(\mathbf{p}) = [h_1(\mathbf{p}), t; t^\dagger, h_2(\mathbf{p})]$. Here $h_l(\mathbf{p})$ are layer-Hamiltonians (layer index $l \in \{1, 2\}$) that can be written as $h_l = h_N(\mathbf{p}) - x(-1)^l h_{\text{AFM}}(\mathbf{p})$ [34, 35]; t describes a \mathbf{p} -independent inter-layer coupling that is PT symmetric, see **SI**.

$h_N(\mathbf{p})$ describes a normal component that is the same in both layers: it is P and T invariant. It takes takes on the familiar BHZ form [36]: $h_N(\mathbf{p}) = \epsilon_0(\mathbf{p})\tau_0\sigma_0 + m(\mathbf{p})\tau_z\sigma_z + \alpha(p_y\tau_0\sigma_x - p_x\tau_0\sigma_y)$ with $\epsilon_0(\mathbf{p})$ and $m(\mathbf{p})$ the dispersive and massive contributions, and α is a velocity. Here τ and σ are Pauli matrices that describe orbital and spin degree of freedom in each layer. In contrast, $h_{\text{AFM}} = \frac{1}{2}\text{diag}[m_1, -m_2, m_2, -m_1]$ captures the Néel order; $x = \pm 1$ captures two distinct antiferromagnetic groundstates with the same energy (see Fig. 2). In-

deed, $-x(-1)^l h_{\text{AFM}}$ breaks P and T symmetry but preserves PT symmetry. $H_0^{\text{MBT}}(\mathbf{p})$ produces a bandstructure that is doubly-degenerate at each \mathbf{p} (Fig. 2 inset). Material parameters can be found in **SI**.

A natural $\hat{O}^{(-)}$ observable in MBT is its layer polarization (LP) [28, 29], $\hat{p}_z = e \cdot \text{diag}[\mathbb{I}_4, -\mathbb{I}_4]$. LP is odd under PT and possesses an expectation value that vanishes in the equilibrium state of PT symmetric MBT. We numerically compute the Kramers nonlinearities described above of LP for H_0^{MBT} in Fig. 2a fixing the Fermi energy in the gap, see **SI** for numerical details. We find KI (blue)/KFS (purple) only manifest as a helicity dependent response described by $\text{Im}[\chi_{\text{LP}}^{xy}(\omega)]$, and display a large and peaked response for frequencies close to transitions about the band extrema. In contrast, the shift-like nonlinear response for LP (shown in red), are almost two orders of magnitude smaller demonstrating the dominant role that KI/KFS play in $\hat{O}^{(-)}$ nonlinearities.

Another natural $\hat{O}^{(-)}$ observable in MBT is spin polarization (SP): $\hat{s}_z = \frac{\hbar}{2} \cdot \text{diag}[\sigma_z\tau_0, \sigma_z\tau_0]$. Similar to LP, Kramers SP nonlinearities are also helicity dependent (red arrows), Fig. 2b. However, unlike SP, $\text{Im}[\chi_{\text{LP}}^{xy}]$ exhibits a Néel order sensitivity, flipping sign when Néel order changes from $x = +1$ to $x = -1$ (Fig. 2b). In contrast, $\text{Im}[\chi_{\text{SP}}^{xy}]$ retains its sign for both Néel orders; instead its sign is locked to the helicity of the incident EM field. This distinction between $\hat{O}^{(-)}$ observables comports with the transformation properties of \hat{p}_z and \hat{s}_z : P flips \hat{p}_z and Néel order but preserves light helicity, while T flips \hat{s}_z , Néel order, as well as light helicity.

Kramers nonlinearities demonstrate the essential role that degeneracy plays in nonlinear response: they vanish in non-degenerate PT symmetric systems and directly depend on the quantum geometry of (Kramers) degenerate bands. We find they dominate the nonlinear response of layer polarization responses in MBT antiferromagnets providing an effective means of identifying the Néel order. For instance, we find large $\text{Im}[\chi_{\text{LP}}^{xy}]$ of order $100\text{e}/\text{V}^2$. Such KI/KFS nonlinearities are orders of

magnitude larger than those recently found for twisted bilayer graphene [29]. Perhaps most striking are the long tails KFS exhibits that extends far below the absorption edge rendering it dissipationless (no absorption required to activate). Dissipationless photocurrent nonlinearities have attracted intense recent interest [6, 32, 37, 38]; however, these require the presence of a Fermi surface making it difficult to isolate from other dissipative processes.

In contrast, KFS appears in insulating antiferromagnets (e.g., MBT) allowing clear means to isolate its presence, as well as a platform for low-dissipation photodetection.

Acknowledgements. We thank Bohm Jung Yang for useful conversations. This work was supported by the Singapore Ministry of Education (MOE) AcRF Tier 2 grant MOE-T2EP50222-0011 and MOE Tier 3 grant MOE 2018-T3-1-002.

-
- [1] M. Z. Hasan and C. L. Kane, *Rev. Mod. Phys.* **82**, 3045 (2010).
- [2] J. J. Sakurai and J. Napolitano, *Modern quantum mechanics* (Cambridge University Press (Virtual Publishing), Cambridge, England, 2020), 3rd ed.
- [3] P. Tang, Q. Zhou, G. Xu, and S.-C. Zhang, *Nature Physics* **12**, 1100 (2016).
- [4] A. Gao, Y.-F. Liu, C. Hu, J.-X. Qiu, C. Tzschaschel, B. Ghosh, S.-C. Ho, D. Bérubé, R. Chen, H. Sun, et al., *Nature* **595**, 521 (2021).
- [5] I. Sodemann and L. Fu, *Physical review letters* **115**, 216806 (2015).
- [6] O. Matsyshyn and I. Sodemann, *Physical review letters* **123**, 246602 (2019).
- [7] J. Sipe and A. Shkrebtii, *Physical Review B* **61**, 5337 (2000).
- [8] F. de Juan, A. G. Grushin, T. Morimoto, and J. E. Moore, *Nature communications* **8**, 1 (2017).
- [9] H. Watanabe and Y. Yanase, *Phys. Rev. X* **11**, 011001 (2021).
- [10] T. Morimoto and N. Nagaosa, *Science advances* **2**, e1501524 (2016).
- [11] J. Ahn, G.-Y. Guo, N. Nagaosa, and A. Vishwanath, *Nature Physics* **18**, 290 (2022).
- [12] J. Ahn, G.-Y. Guo, and N. Nagaosa, *Phys. Rev. X* **10**, 041041 (2020).
- [13] Y. Onishi and L. Fu, *Phys. Rev. X* **14**, 011052 (2024).
- [14] T. Neupert, C. Chamon, and C. Mudry, *Phys. Rev. B* **87**, 245103 (2013).
- [15] D. Xiao, M.-C. Chang, and Q. Niu, *Rev. Mod. Phys.* **82**, 1959 (2010).
- [16] N. Verma and R. Queiroz, *Instantaneous response and quantum geometry of insulators* (2024), 2403.07052.
- [17] J.-W. Rhim, K. Kim, and B.-J. Yang, *Nature* **584**, 59 (2020).
- [18] J. P. Provost and G. Vallee, *Communications in Mathematical Physics* **76**, 289 (1980).
- [19] H. Wang and X. Qian, *Science Advances* **5**, eaav9743 (2019).
- [20] T. Holder, D. Kaplan, and B. Yan, *Phys. Rev. Res.* **2**, 033100 (2020).
- [21] N. Wang, D. Kaplan, Z. Zhang, T. Holder, N. Cao, A. Wang, X. Zhou, F. Zhou, Z. Jiang, C. Zhang, et al., *Nature* **621**, 487 (2023).
- [22] J.-X. Qiu, C. Tzschaschel, J. Ahn, A. Gao, H. Li, X.-Y. Zhang, B. Ghosh, C. Hu, Y.-X. Wang, Y.-F. Liu, et al., *Nature Materials* **22**, 583 (2023).
- [23] J. Godinho, H. Reichlova, D. Kriegner, V. Novak, K. Olejnik, Z. Kaspar, Z. Soban, P. Wadley, R. P. Campion, R. M. Otxoa, et al., *Nature Communications* **9**, 4686 (2018).
- [24] Y. Xiang, W. Huang, L. Tan, T. Chen, Y. He, P. S. Irving, K. M. Weeks, Q. C. Zhang, and X. Dong, *Nature* **621**, 423 (2023).
- [25] B. M. Fregoso, *Phys. Rev. B* **100**, 064301 (2019).
- [26] D. E. Parker, T. Morimoto, J. Orenstein, and J. E. Moore, *Phys. Rev. B* **99**, 045121 (2019).
- [27] D. Rees, K. Manna, B. Lu, T. Morimoto, H. Borrmann, C. Felser, J. E. Moore, D. H. Torchinsky, and J. Orenstein, *Science Advances* **6**, eaba0509 (2020).
- [28] O. Matsyshyn, Y. Xiong, A. Arora, and J. C. W. Song, *Phys. Rev. B* **107**, 205306 (2023).
- [29] Y. Gao, Y. Zhang, and D. Xiao, *Phys. Rev. Lett.* **124**, 077401 (2020).
- [30] Q. Ma, R. Krishna Kumar, S.-Y. Xu, F. H. L. Koppens, and J. C. W. Song, *Nature Reviews Physics* **5**, 170 (2023).
- [31] P. Törmä, *Phys. Rev. Lett.* **131**, 240001 (2023).
- [32] O. Matsyshyn, J. C. Song, I. S. Villadiego, and L.-k. Shi, *Physical Review B* **107**, 195135 (2023).
- [33] F. de Juan, Y. Zhang, T. Morimoto, Y. Sun, J. E. Moore, and A. G. Grushin, *Phys. Rev. Res.* **2**, 012017 (2020).
- [34] B. Lian, Z. Liu, Y. Zhang, and J. Wang, *Phys. Rev. Lett.* **124**, 126402 (2020).
- [35] A. Gao, Y.-F. Liu, J.-X. Qiu, B. Ghosh, T. V. Trevisan, Y. Onishi, C. Hu, T. Qian, H.-J. Tien, S.-W. Chen, et al., *Science* **381**, 181 (2023).
- [36] B. A. Bernevig and T. L. Hughes, *Topological Insulators and Topological Superconductors* (Princeton University Press, 2013).
- [37] L.-k. Shi, O. Matsyshyn, J. C. Song, and I. S. Villadiego, *Physical Review B* **107**, 125151 (2023).
- [38] T. G. Rappoport, T. A. Morgado, S. Lannebère, and M. G. Silveirinha, *Phys. Rev. Lett.* **130**, 076901 (2023).

Supplementary Information

A. Injection nonlinearity and dynamics in a Kramers degenerate system

In this section, we derive the injection nonlinearity in Eq. (4) for a Kramers degenerate system. As discussed in the main text, we consider a doubly degenerate Bloch electronic system $H_0(\mathbf{p})$ irradiated by a monochromatic EM field $\mathbf{E}(t) = \frac{1}{2}(\mathbf{E}_\omega e^{-i\omega t} + c.c.)$. In dipole approximation, the light-matter interaction can be captured by $\hat{V}(t) = e\mathbf{E}(t) \cdot \hat{\mathbf{r}} e^{\eta t/\hbar}$, where e is the charge, and $\eta \rightarrow 0^+$ is an adiabatic turn-on parameter. As we now show, the EM field can induce vertical interband transitions satisfying energy and momentum conservation, as well as coherence between in Kramers pairs. Importantly, the perturbed state is a superposition of both the Kramers pairs in the valence band $\{|u_v(\mathbf{p})\rangle, |u_{\bar{v}}(\mathbf{p})\rangle\}$ and the conduction band $\{|u_c(\mathbf{p})\rangle, |u_{\bar{c}}(\mathbf{p})\rangle\}$, see Eq. (3) in the main text, where the coefficients $s_j(t)$ (where $j \in \{v, \bar{v}, c, \bar{c}\}$) can be solved from the time dependent Schrödinger equation $H\psi(t) = i\hbar\partial_t\psi(t)$:

$$\dot{s}_j(t) = -\frac{i}{\hbar} \sum_i s_i(t) V_{ji}(t) e^{i\omega_{ji}t}, \quad (\text{S1})$$

where $\omega_{ij} = [\epsilon_i(\mathbf{p}) - \epsilon_j(\mathbf{p})]/\hbar$, and $V_{ij} = \langle u_i(\mathbf{p}) | \hat{V}(t) | u_j(\mathbf{p}) \rangle$ is the light-matter interaction matrix element.

We first consider an initial electronic state $|u_v(\mathbf{p})\rangle$ such that $s_v(t_0) = 1$ and $s_{\bar{v}}(t_0) = s_{c,\bar{c}}(t_0) = 0$. Solving Eq. (S1) iteratively up to the order V^2 and taking $t_0 \rightarrow -\infty$, we find that for the conduction band $j \in \{c, \bar{c}\}$, $s_j(t)$ contains a first order correction:

$$s_j(t) = -V_{jv}(\omega) \frac{e^{i(\omega_{jv}-\omega)t+\eta t/\hbar}}{\epsilon_{jv} - \hbar\omega - i\eta} + (\omega \leftrightarrow -\omega), \quad (\text{S2})$$

where $V_{ji}(\omega) = \langle u_j(\mathbf{p}) | \hat{V}_\omega | u_i(\mathbf{p}) \rangle$ and $\hat{V}_\omega = e\mathbf{E}_\omega \cdot \hat{\mathbf{r}}$. Furthermore, the Kramers pair in the valence band contains a second order correction. For $j \in \{v, \bar{v}\}$, we have (neglecting terms oscillating faster than ω)

$$s_j(t) = s_j(t_0) + i \sum_i \frac{V_{ji}(-\omega)V_{iv}(\omega)e^{2\eta t/\hbar}}{2\eta(\epsilon_{ij} - \hbar\omega - i\eta)} + (\omega \leftrightarrow -\omega). \quad (\text{S3})$$

The expectation value of observable O can be directly computed $\langle O \rangle = \langle \psi(t) | \hat{O} | \psi(t) \rangle$ after summing over all initial states $\{v, \bar{v}\}$. For electronic transitions from the set of degenerate states $\{v, \bar{v}\}$ to $\{c, \bar{c}\}$, the second order response of \hat{O} is given by

$$O_{\{v, \bar{v}\} \rightarrow \{c, \bar{c}\}} = \sum_{\zeta=\pm, a, b} \frac{e^{2\pi} e^{2\eta t/\hbar}}{4\eta} \delta(\epsilon_{cv} - \zeta\hbar\omega) r_{vc}^\alpha \left[\sum_{i, \epsilon_i = \epsilon_c} O_{ci} r_{iv}^\beta - \sum_{j, \epsilon_j = \epsilon_v} O_{jv} r_{cj}^\beta \right] E_{-\zeta\omega}^\alpha E_{\zeta\omega}^\beta. \quad (\text{S4})$$

In a system with chemical potential μ and temperature T , the transition rates depend on the electronic occupation functions of the initial and final states. As a result, the second order response due to transitions from the valence band to the conduction band is

$$O_{\text{val} \rightarrow \text{cond}} = \sum_{\zeta=\pm, \alpha, \beta} \int_{\mathbf{p}} \frac{e^{2\pi} e^{2\eta t/\hbar}}{4\eta} \delta(\epsilon_{cv} - \zeta\hbar\omega) f[\epsilon_v(\mathbf{p})] \{1 - f[\epsilon_c(\mathbf{p})]\} r_{vc}^\alpha \left[\sum_{i, \epsilon_i = \epsilon_c} O_{ci} r_{iv}^\beta - \sum_{j, \epsilon_j = \epsilon_v} O_{jv} r_{cj}^\beta \right] E_{-\zeta\omega}^\alpha E_{\zeta\omega}^\beta. \quad (\text{S5})$$

Similarly, the second order response due to transitions from the conduction band to the valence band is

$$O_{\text{cond} \rightarrow \text{val}} = \sum_{\zeta=\pm, \alpha, \beta} \int_{\mathbf{p}} \frac{e^{2\pi} e^{2\eta t/\hbar}}{4\eta} \delta(\epsilon_{vc} - \zeta\hbar\omega) f[\epsilon_c(\mathbf{p})] \{1 - f[\epsilon_v(\mathbf{p})]\} r_{cv}^\alpha \left[\sum_{i, \epsilon_i = \epsilon_v} O_{vi} r_{ic}^\beta - \sum_{j, \epsilon_j = \epsilon_c} O_{jc} r_{vj}^\beta \right] E_{-\zeta\omega}^\alpha E_{\zeta\omega}^\beta. \quad (\text{S6})$$

The total second order response associated with \hat{O} is obtained by summing over all transitions in Eq. (S5) and Eq. (S6). After taking a time derivative, we arrive at the injection nonlinearity in Eq. (4) of the main text:

$$\frac{dO}{dt} = \sum_{\zeta=\pm, \alpha, \beta} \int_{\mathbf{p}} \frac{e^{2\pi}}{2\hbar} \delta(\epsilon_{cv} - \zeta\hbar\omega) f_{vc} r_{vc}^\alpha \left[\sum_{i, \epsilon_i = \epsilon_c} O_{ci} r_{iv}^\beta - \sum_{j, \epsilon_j = \epsilon_v} O_{jv} r_{cj}^\beta \right] E_{-\zeta\omega}^\alpha E_{\zeta\omega}^\beta. \quad (\text{S7})$$

While we have derived the Kramers injection nonlinearity via the time-dependent perturbation theory, Eq. (4) can be reproduced from a more systematic approach using the quantum Liouville equation as discussed below.

Additionally, by considering the PT transformation properties for r_{nm}^α and \mathbb{O}_{mn}^β , explicitly written in the main text, Eq. (4) can be shown to be proportional to $E_{-\omega}^\alpha E_\omega^\beta - E_\omega^\alpha E_{-\omega}^\beta = \varepsilon^{\alpha\beta\gamma} d^\gamma$, where $d^\gamma = [\mathbf{E}_{-\omega} \times \mathbf{E}_\omega]^\gamma$.

B. Systematic quantum Liouville approach for nonlinear response

In order to systematically derive the optical response of an electronic insulator (being careful to include the effects of Kramers degeneracy), we perturbatively solve the Liouville equation $i\hbar d_t \hat{\rho}(\mathbf{k}, t) = [\hat{H}_0(\mathbf{k}) + \hat{V}(\mathbf{k}, t), \hat{\rho}(\mathbf{k}, t)]$, assuming that in equilibrium Bloch states are thermally populated $\langle n(\mathbf{k}) | \hat{\rho}_{\text{eq}}(\mathbf{k}) | m(\mathbf{k}) \rangle = f_{\text{FD}}[\epsilon_n(\mathbf{k})] \delta_{nm}$. Here $\hat{\rho}(\mathbf{k}, t)$ is the density matrix. At second order, the correction to the rectified density matrix is

$$\hat{\rho}_{mn}^{(2)} = e^{2\eta t/\hbar} \frac{e^2}{\hbar^2} \int \frac{d\omega}{2\pi} E_{-\omega}^\alpha E_\omega^\beta \left[\frac{1}{\epsilon_{nm} + 2i\eta} i\partial_k^\alpha \frac{A_{mn}^\beta f_{nm}}{\hbar\omega - \epsilon_{mn} + i\eta} + \frac{1}{\epsilon_{nm} + 2i\eta} \sum_c \left\{ \frac{A_{mc}^\alpha A_{cn}^\beta f_{nc}}{\hbar\omega - \epsilon_{cn} + i\eta} - \frac{A_{mc}^\beta A_{cn}^\alpha f_{cm}}{\hbar\omega - \epsilon_{mc} + i\eta} \right\} \right]. \quad (\text{S8})$$

The nonlinear rectified response of any observable O represented by an operator \hat{O} is given by $\langle O \rangle = \sum_{p,nm} O_{nm} \rho_{mn}$. We write such explicitly by contracting Eq.(S8) with O_{nm} to find:

$$O_{\text{inter}}^{(2)} = e^{2\eta t/\hbar} \int_{\mathbf{p}} \sum_{nm} \int \frac{d\omega}{2\pi} E_{-\omega}^\alpha E_\omega^\beta \left[\frac{O_{nm}}{\epsilon_{nm} + 2i\eta} i\partial_k^\alpha \frac{A_{mn}^\beta f_{nm}}{\hbar\omega + \epsilon_{nm} + i\eta} + \frac{A_{mn}^\beta f_{nm}}{\hbar\omega + \epsilon_{nm} + i\eta} \sum_c \left\{ \frac{O_{nc} A_{cm}^\alpha}{\epsilon_{nc} + 2i\eta} - \frac{A_{nc}^\alpha O_{cm}}{\epsilon_{cm} + 2i\eta} \right\} \right]. \quad (\text{S9})$$

We note that when expressing the nonlinear susceptibility tensor $\chi^{\alpha\beta}(\omega)$, there is a ‘‘gauge’’ freedom. This is because when $\chi^{\alpha\beta}(\omega)$ contracted with a pair of electric fields, the physical response is symmetric under $\alpha \leftrightarrow \beta, \omega \leftrightarrow -\omega$:

$$\sum_{\alpha\beta} \int \frac{d\omega}{2\pi} E_{-\omega}^\alpha E_\omega^\beta \chi^{\alpha\beta}(\omega) = \frac{1}{2} \sum_{\alpha\beta} \int \frac{d\omega}{2\pi} E_{-\omega}^\alpha E_\omega^\beta (\chi^{\alpha\beta}(\omega) + \chi^{\beta\alpha}(-\omega)). \quad (\text{S10})$$

In what follows, as well as in the main text, we write the susceptibility tensors in a *symmetrized* form.

1. Kramers nonlinearities

The different terms of Eq.(S9) represent distinct nonlinearities. We first focus on the second term in the square brackets of Eq.(S9). Importantly, first term in curly brackets when $\epsilon_c = \epsilon_n$ and second term for $\epsilon_c = \epsilon_m$ are proportional to $1/\eta$. For small η these terms are large. As we will now see, these terms form Kramers nonlinearities. Focusing on these nonlinear response terms in Eq.(S9) and writing them in a *symmetrized* form, we obtain

$$O_{\text{Kramers}}^{(2)} = \frac{1}{2} e^{2\eta t/\hbar} \int_{\mathbf{p}} \sum_{nm} \int \frac{d\omega}{2\pi} E_{-\omega}^\alpha E_\omega^\beta \left[\frac{A_{mn}^\beta f_{mn}}{(\hbar\omega + \epsilon_{nm})^2 + \eta^2} \left\{ \sum_{c, \epsilon_c = \epsilon_n} O_{nc} A_{cm}^\alpha - \sum_{c, \epsilon_c = \epsilon_m} A_{nc}^\alpha O_{cm} \right\} \right]. \quad (\text{S11})$$

Next we observe the following identity:

$$\lim_{\eta \rightarrow 0} \frac{1}{(\hbar\omega + \epsilon_{nm})^2 + \eta^2} = \lim_{\eta \rightarrow 0} \frac{\eta^2}{((\hbar\omega + \epsilon_{nm})^2 + \eta^2)^2} + \lim_{\eta \rightarrow 0} \frac{(\omega + \epsilon_{nm})^2}{((\hbar\omega + \epsilon_{nm})^2 + \eta^2)^2} = \frac{\pi}{2\eta} \delta(\hbar\omega + \epsilon_{nm}) + \mathcal{P} \frac{1}{(\hbar\omega + \epsilon_{nm})^2}, \quad (\text{S12})$$

Applying the above identity to Eq. (S11) we obtain the Kramers Injection (KI) nonlinearity as

$$O_{\text{KI}}^{(2)} = \frac{\pi}{4\eta} e^{2\eta t/\hbar} \int_{\mathbf{p}} \sum_{nm} \int \frac{d\omega}{2\pi} E_{-\omega}^\alpha E_\omega^\beta \delta(\hbar\omega + \epsilon_{nm}) A_{mn}^\beta f_{mn} \left\{ \sum_{c, \epsilon_c = \epsilon_n} O_{nc} A_{cm}^\alpha - \sum_{c, \epsilon_c = \epsilon_m} A_{nc}^\alpha O_{cm} \right\}, \quad (\text{S13})$$

and Kramers Fermi Sea (KFS) nonlinearity as

$$O_{\text{KFS}}^{(2)} = \frac{1}{2} e^{2\eta t/\hbar} \int_{\mathbf{p}} \sum_{nm} \int \frac{d\omega}{2\pi} E_{-\omega}^\alpha E_\omega^\beta \mathcal{P} \frac{A_{mn}^\beta f_{mn}}{(\hbar\omega + \epsilon_{nm})^2} \left\{ \sum_{c, \epsilon_c = \epsilon_n} O_{nc} A_{cm}^\alpha - \sum_{c, \epsilon_c = \epsilon_m} A_{nc}^\alpha O_{cm} \right\}. \quad (\text{S14})$$

Note that taking a time derivative of the Kramers injection nonlinearity in Eq. (S13) in the limit of $\eta \rightarrow 0$ yields Eq. (4) of the main text. This corresponds to the resonant (absorptive) part of of Eq. (S11). As we will see below, by using the λ -formulation before, the quantum geometric content of Eq. (S13) revealed producing Eq. (6) of the main text.

Eq. (S14) corresponds to the off-resonant component of Eq.(S11) and arises even in the absence of any absorption. By using the λ -formulation, this KFS nonlinearity in Eq. (S14) produces Eq. (8) of the main text. The above forms are numerically friendly, and was employed to produce Fig. 2 of the main text.

2. Shift-like nonlinearities

Considering the rest of the terms in Eq.(S9) we find the Shift-like nonlinearities. After integrating by parts for ∂_k^α in Eq.(S9), we find these nonlinearities are naturally grouped as:

$$\delta O_{\text{Shift-like}}^{(2)} = e^{2\eta t/\hbar} \int_{\mathbf{p}} \sum_{nm} \int \frac{d\omega}{2\pi} E_{-\omega}^\alpha E_\omega^\beta \frac{iA_{mn}^\beta f_{mn}}{\hbar\omega + \epsilon_{nm} + i\eta} \left[\partial^\alpha \frac{O_{nm}}{\epsilon_{nm}} - i \left\{ \sum_{c, \epsilon_c \neq \epsilon_m} A_{nc}^\alpha \frac{O_{cm}}{\epsilon_{cn}} - \sum_{c, \epsilon_c \neq \epsilon_n} \frac{O_{nc}}{\epsilon_{nc}} A_{cm}^\alpha \right\} \right]. \quad (\text{S15})$$

Using identity: $\lim_{\eta \rightarrow 0} 1/(x + i\eta) = \text{P}(1/x) - i\pi\delta(x)$, Eq.(S15) can be similarly be separated into the resonant and off-resonant components. We note the numerically friendly form of the expression in the brackets is:

$$\begin{aligned} \partial_k^\beta \frac{O_{mn}}{\epsilon_{mn}} - i \left[\sum_{c, \epsilon_c \neq \epsilon_n} A_{mc}^\beta \frac{O_{cn}}{\epsilon_{cn}} - \sum_{c, \epsilon_c \neq \epsilon_m} \frac{O_{mc}}{\epsilon_{mc}} A_{cn}^\beta \right] &= \\ &= \frac{1}{\epsilon_{mn}} \langle m | \frac{\partial \hat{O}}{\partial k^\beta} | n \rangle + \frac{1}{\epsilon_{mn}^2} \left[\sum_{c, \epsilon_c = \epsilon_n} v_{mc}^\beta O_{cn} - \sum_{c, \epsilon_c = \epsilon_m} v_{cn}^\beta O_{mc} \right] + \frac{1}{\epsilon_{mn}} \left[\sum_{c, \epsilon_c \neq \epsilon_m} \frac{O_{mc} v_{cn}^\beta}{\epsilon_{mc}} - \sum_{c, \epsilon_c \neq \epsilon_n} \frac{v_{mc}^\beta O_{cn}}{\epsilon_{cn}} \right]. \end{aligned} \quad (\text{S16})$$

C. Kramers quantum geometry and λ -formulation

In this section we massage the KI, KFS and shift-like nonlinearities to their compact geometrical form as shown in the main text. As in the main text, we examine the set of parametric Hamiltonians $H_{\text{eff}}(\lambda, \mathbf{p}) = H_0(\mathbf{p}) + \lambda \hat{O}^{(-)}$, allowing us to write $\hat{O}^{(-)} = \partial H_{\text{eff}} / \partial \lambda$, with the matrix elements as in Eq.(5) of the main text.

It is important to note, that the λ -term lifts the exact PT symmetry protected degeneracy of Kramers states, since $\hat{O}^{(-)}$ is PT-odd. In order to explicitly track the states that in the limit of $\lambda \rightarrow 0$ become Kramers degenerate, it is useful to denote such states via $\epsilon_n \approx \epsilon_c$. Naturally, in the limit $\lambda \rightarrow 0$, the exact degeneracy of the equality is restored $\approx \rightarrow =$. Using this notation we write the Kramers nonlinearities as:

$$\delta O_{\text{Kramers}}^{(2)} = \frac{1}{2} e^{2\eta t/\hbar} \int_{\mathbf{p}} \sum_{nm} \int \frac{d\omega}{2\pi} E_{-\omega}^\alpha E_\omega^\beta \left[\frac{A_{mn}^\beta f_{mn}}{(\hbar\omega + \epsilon_{nm})^2 + \eta^2} \left\{ \sum_{c, \epsilon_c \approx \epsilon_n} O_{nc} A_{cm}^\alpha - \sum_{c, \epsilon_c \approx \epsilon_m} A_{nc}^\alpha O_{cm} \right\} \right]. \quad (\text{S17})$$

Employing the covariant derivative with respect to λ as:

$$S_{mn}^{\alpha; \lambda} = \nabla_\lambda S_{mn}^\alpha = \partial^\lambda S_{mn}^\alpha - i \left[\sum_{c, \epsilon_c \approx \epsilon_m} A_{mc}^\lambda S_{cn}^\alpha - \sum_{c, \epsilon_c \approx \epsilon_n} S_{mc}^\alpha A_{cn}^\lambda \right], \quad (\text{S18})$$

we can to find the following identity:

$$\nabla_\lambda v_{nm}^\alpha - i \epsilon_{nm} \nabla_\lambda A_{nm}^\alpha = i \sum_{c, \epsilon_c \approx \epsilon_n} O_{nc} A_{cm}^\alpha - i \sum_{c, \epsilon_c \approx \epsilon_m} A_{nc}^\alpha O_{cm}. \quad (\text{S19})$$

After substitution of Eq.(S19) into Eq.(S17) and using Eq.(S12) we find the KI and KFS responses displayed in the main text.

Finally, using the fact that $\sum_{c, \epsilon_c \neq \epsilon_n} = \sum_c - \sum_{c, \epsilon_c \approx \epsilon_n}$, and the following identity for the Berry connections: $\partial_k^\alpha A_{nm}^\lambda - i \sum_c [A_{nc}^\alpha A_{cm}^\lambda - A_{nc}^\lambda A_{cm}^\alpha] = \partial^\lambda A_{nm}^\alpha$, we can rewrite shift-like nonlinearities as:

$$\begin{aligned} \delta O_{\text{Shift-like}}^{(2)} &= \frac{1}{2} e^{2\eta t/\hbar} \int_{\mathbf{p}} \sum_{nm} \int \frac{d\omega}{2\pi} E_{-\omega}^\alpha E_\omega^\beta \pi \delta(\hbar\omega + \epsilon_{nm}) f_{mn} i (A_{nm}^{\alpha; \lambda} A_{mn}^\beta - A_{nm}^\alpha A_{mn}^{\beta; \lambda}) \\ &\quad + \frac{1}{2} \int_{\mathbf{p}} \sum_{nm} \int \frac{d\omega}{2\pi} E_{-\omega}^\alpha E_\omega^\beta (A_{nm}^{\alpha; \lambda} A_{mn}^\beta + A_{nm}^\alpha A_{mn}^{\beta; \lambda}) \mathcal{P} \frac{f_{nm}}{\hbar\omega + \epsilon_{nm}}. \end{aligned} \quad (\text{S20})$$

Much like Eq. (6), the shift-like nonlinearities in Eq. (S20) depends on a generalized covariant derivative that includes the Kramers pairs. However, unlike Eq. (6), Eq. (S20) can be non-vanishing for PT-symmetric non-degenerate energy bands only leading to the restriction $\chi_{\text{shift FS}}^{\alpha\beta}(\omega) = \chi_{\text{shift FS}}^{\beta\alpha}(\omega) = \chi_{\text{shift FS}}^{\alpha\beta}(-\omega)$.

D. MBT Hamiltonian

In our numerical calculations of nonlinearities of MBT, we adopted low energy effective Hamiltonian [34, 35], with the normal and AFM components of the Hamiltonian in the spin-orbital basis $(|p_{z,\text{Bi}}^+, \uparrow\rangle, |p_{z,\text{Te}}^-, \downarrow\rangle, |p_{z,\text{Te}}^-, \uparrow\rangle, |p_{z,\text{Bi}}^+, \downarrow\rangle)^T$. Explicitly the normal components of the Hamiltonian and the interlayer couplings are:

$$h_N(\mathbf{k}) = \epsilon_0(\mathbf{k})\mathbb{I}_4 + \begin{pmatrix} m(\mathbf{k}) & i\alpha k_- & & \\ -i\alpha k_+ & -m(\mathbf{k}) & & \\ & & -m(\mathbf{k}) & i\alpha k_- \\ & & -i\alpha k_+ & m(\mathbf{k}) \end{pmatrix}, \quad t = \begin{pmatrix} t_1 & 0 & -\lambda & 0 \\ 0 & t_2 & 0 & \lambda \\ \lambda & 0 & t_2 & 0 \\ 0 & -\lambda & 0 & t_1 \end{pmatrix} \quad (\text{S21})$$

with $k_{\pm} = k_x \pm ik_y$, the dispersive part $\epsilon_0(\mathbf{k}) = \gamma_0 + \gamma k^2$, and massive part $m(\mathbf{k}) = m_0 + \beta_0 k^2$. The set of parameters adopted were extracted from Ref.[35] that was recently used to successfully capture the effective electronic behavior of antiferromagnetic even MBT layers. For the convenience of the reader, we the parameters are as follows: $\gamma = 17.0 \text{ eV} \cdot \text{\AA}^2, m_0 = -0.04 \text{ eV}, \beta_0 = 9.40 \text{ eV} \cdot \text{\AA}^2, \alpha = 3.20 \text{ eV} \cdot \text{\AA}, m_1 = 0.05 \text{ eV}, m_2 = 0.09 \text{ eV}, t_1 = -0.0533 \text{ eV}, t_2 = 0.0463 \text{ eV}, \lambda = 0.0577 \text{ eV}$.